Dalton Transactions

ROYAL SOCIETY OF CHEMISTRY

PAPER

View Article Online
View Journal | View Issue

Cite this: *Dalton Trans.*, 2024, **53**, 8608

Transition metal and lanthanide modified MOF-808 for barcode design†

Nele Marquardt, Frederike von der Haar and Andreas Schaate *

This study explores the utilization of metal–organic frameworks (MOFs), particularly those incorporating lanthanide-based elements for their fluorescence capabilities, to create an advanced barcode system. By exploiting the modular nature of MOFs, we have developed a material capable of dynamic information encoding and robust against counterfeiting efforts. We introduce a novel barcode prototype that exhibits visible color shifts and fluorescence modulation when exposed to a specific sequence of chemical and thermal stimuli. The barcode is composed of MOF-808, which is modified with transition metals like iron or cobalt, and europium cations. These components are embedded within polyvinylidene fluoride (PVDF) to form a composite. This embedding process ensures that the MOF particles remain reactive to specific trigger molecules, enabling a distinct read-out sequence. The decoding process, involving exposure to ammonia, heating at 120 °C, and treatment with HCl, triggers observable changes in fluorescence and color, depending on the transition metal used. Our investigations with Eu,Co-MOF-808, and Eu,Fe-MOF-808 composites have resulted in the creation of a barcode prototype that demonstrates the feasibility of using europium-modified and unmodified transition metal modified MOF-808@PVDF composites for enhanced security applications.

Received 20th February 2024,
Accepted 24th April 2024

DOI: 10.1039/d4dt00501e

rsc.li/dalton

1. Introduction

Barcodes have become an indispensable part of everyday life, not only for the identification and marking of goods, but also for the encoding of personal data. Accordingly, the encoded data is becoming increasingly sensitive, ranging from secure product authentication to the protection of confidential information. As the reliance on barcodes for various applications continues to grow, so does the need to develop forgery-proof barcodes.

Materials with characteristic fluorescence properties that can be specifically altered by stimulation of external factors such as temperature or chemicals are popular for the design of anti-counterfeit barcodes.[1] Most commonly, lanthanide-based materials[2] are used for this application because they have many advantages over other luminescent materials like sharp emission, broad excitation spectra and low toxicity.[3]

Metal–organic frameworks (MOFs) are a promising class of materials for the design of lanthanide-based fluorescent barcodes. Due to their modular structure, there are many possibilities to incorporate lanthanides into the framework. The incorporation is not only possible by the formation of so-called Ln-MOFs with lanthanide-based inorganic building units (IBUs),[4] but also by the post-synthetic coordination of the cations to functionalities of linker molecules[5] or to open metal sites at the IBUs.[6] Furthermore, aromatic linker molecules allow the sensitization of the luminescence of lanthanide cations, thus they can act as antenna molecules.[7]

Many MOF-based barcodes show a fine-tuned fluorescence as read-out response by the simultaneous emission of several independent signals resulting from different lanthanide ions incorporated in the same material. The fluorescence response of the polymetallic MOFs with controlled compositions can be located in the visible[5] as well as in the NIR range[8] depending on the lanthanides used. Deneff *et al.*[9] have combined visible and NIR emitting lanthanide cations in the same Ln-MOF to obtain a material with an overt and covert signature that can be obtained by direct excitation of the respective lanthanides. In addition, the tunable fluorescence lifetime of the compounds allows for a second encoding, resulting in a higher level of security.

There are also reports of Ln-MOFs exhibiting switchable fluorescence induced by external stimuli, which represents another possibility to achieve a higher level of forgery protection. Gao *et al.*[10] present a responsive photonic barcode based on multicolor Ln-MOF heterostructures prepared by

Institute of Inorganic Chemistry, Leibniz University Hannover, Callinstr. 9, 30167 Hannover, Germany. E-mail: andreas.schaate@acb.uni-hannover.de; Fax: +49511 762 3660; Tel: +49 511 762 3698

† Electronic supplementary information (ESI) available. See DOI: https://doi.org/10.1039/d4dt00501e

integrating multi-responsive MOF blocks into a single microstructure by a stepwise epitaxial growth. The fluorescence response can be thermally switched due to the ability of energy transfer between the incorporated terbium cations to europium cations, which is favored at higher temperatures, causing a stepwise transition from green to red with increasing temperature.

In addition to thermal treatment, chemical treatment is also a widely used tool for the encoding of the real information. The same group forms a composite material containing Eu-MOF and nitrogen and sulfur co-doped carbon dots to generate dual-emission centers.[11] The real information can be encoded by quenching the characteristic red emission of the Eu-MOF in acidic environment, which causes the appearance of the fluorescence of the carbon dots. The real information can be recovered in alkaline environment.

Apart from this one-step decoding, Zhang *et al.*[12] present a multi-step read-out sequence of their Ln-MOF, which exhibits multiple fluorescence colors. The sequence is based on the improvement or deterioration of the energy transfer from the antenna molecule to the incorporated lanthanides induced by copper cations and anticancer drugs, causing the *turn-on* or *turn-off* of the lanthanide-induced fluorescence while preserving that of the linker molecule or inducing the total *turn-off*, depending on the anticancer drug used.

The zirconium-based MOF-808 exhibits high thermal and chemical stability combined with a high porosity and diverse modification possibilities because its IBUs are only half saturated by linker molecules.[13] The remaining coordination sites can be saturated by different monocarboxylic acids[14] or metals such as transition metals like iron[15] and lanthanides like europium[16] and terbium.[6]

The installation of the mentioned metal cations at the oxygen atoms of the IBUs of MOF-808 was confirmed by extended X-ray absorption fine structure (EXAFS) and X-ray absorption near edge spectroscopy (XANES).[6,17] If iron(II) chloride is used for modification, the main present species are Fe-oxo dimers bridging two neighboring Zr_6O_8 nodes, which was analyzed by synchrotron XAFS and pair distribution function (PDF) characterization in combination with DFT modelling.[15] In addition, transition metal and lanthanide cations have already been installed on the same zirconium oxo clusters that comprise a $[Zr_6^{IV}Fe_2^{III}Ln_2^{III}O_8]$ metal oxo core. The structure of the clusters was elucidated from single-crystal diffraction data.[18]

In this work, we want to tackle an important question: How can we create barcodes that are highly resistant to counterfeiting while enabling dynamic information encoding? To address this, we present a forgery-proof barcode prototype that exhibits both visible color change and fluorescence switching triggered by a defined multi-step read-out sequence including chemical and thermal stimuli. The barcode is based on MOF-808 modified with transition metals such as iron or cobalt and europium cations to combine both optical properties, color and fluorescence, in the same material.

2. Experimental

2.1 Synthesis of MOF-808

The synthesis of water-based MOF-808 was performed in round-bottom flasks under reflux conditions and stirring using a modified approach published before.[19,20]

$ZrCl_4$ (30 mmol, 1 eq.) and H_3btc (10 mmol, 0.33 eq.) were dissolved in a mixture of concentrated HCl (1 mL, 0.4 eq.), acetic acid (50 mL, 26.9 eq.), and water (100 mL, 184.7 eq.). The mixture was then heated in an oil bath at110 °C for 24 h. The resulting white MOF-808 powder was isolated by centrifugation (6000 rpm, 10 min) and washed three times with water and two times with acetone. The powder was pre-dried at 60 °C for at least 2 h and further drying was performed at 120 °C.

2.2 Post-synthetic modification of MOF-808 with transition metals

The incorporation of transition metals was performed in DMF. $CoCl_2{\cdot}6H_2O$ or $FeCl_2{\cdot}4H_2O$ (1 eq.), respectively, was dissolved in DMF (333 mL) by ultrasonication. MOF-808-AA (5 g, 0.167 eq.) was added to the resulting blue or orange-brown solution, and the mixture was heated at 60 °C in an oven for 24 h. The powders obtained were isolated by centrifugation (6000 rpm, 10 min), washed with DMF until the supernatant became colorless and then once with acetone. The final products, blue or orange-brown in color, were dried at 60 °C.

2.3 Post-synthetic modification of MOF-808 and TM-MOF-808 with europium

The insertion of europium was performed in acetone at room temperature. Initially, $Eu(NO)_3{\cdot}6H_2O$ (1 eq.) was dissolved in acetone (33.3 mL) by ultrasonication. Then, MOF-808 or TM-MOF-808 (TM = Co or Fe, 500 mg, 0.167 eq.) were added to the colorless solution. After 24 h, the powders were isolated by centrifugation (6000 rpm, 10 min), washed three times with acetone for Eu-MOF-808-AA and continuous washing until colorless supernatant for TM-MOF-808. The powders were dried at 60 °C. Eu-MOF-808-AA was obtained as a white powder, Eu,Co-MOF-808-AA as a bluish powder and Eu,Fe-MOF-808-AA as an orange powder.

2.4 Preparation of mixed-matrix membranes

Mixed-matrix membranes (MMMs) were prepared following a procedure described in the literature.[21] Initially, the MOF ink was produced for a 60 wt% MMM by dispersing TM-MOF-808 (480 mg) in 20 mL acetone by sonication for 30 min. Meanwhile, 321 mg of PVDF were dissolved in 4.16 mL DMF with gentle heating and stirring. This solution was then added to the MOF dispersion and further sonicated for additional 30 min. Afterwards, acetone was removed by rotary evaporation. The ink was manually applied to a glass slide using a 400 μm doctor blade. The films were then heated to 70 °C in an oven without circulating air for 1 h to evaporate the remaining solvent. After this procedure, the MMMs, designated as TM-MOF-808@PVDF, delaminated from the substrate.

2.5 Synthesis of Eu,TM-MOF-808@PVDF

Before the modification with europium cations, the MMMs were cut into 1 cm × 1 cm squares. A single square was soaked in a solution of europium(III)-nitrate and acetone (28 mg Eu $(NO_3)_3 \cdot 6H_2O$ in 1 mL acetone) for 10 min. Following this, the square was washed several times with acetone to remove excess europium salt and transition metals that may have been extracted during the modification procedure. Eu, TM-MOF-808@PVDF was dried at 60 °C in an oven.

2.6 Read-out sequence

The read-out sequence involved placing approximately 150 mg of the powders or four pieces of MMMs on a Petri dish inside a crystallization dish. Every read-out step was performed for a time period of 1 h for the powder samples and 10 min for the MMMs. In the first step, a screw lid glass containing NH_3 solution was placed into the crystallization dish, which was then covered to create a NH_3 atmosphere. For the second step, the samples were removed from this atmosphere and either 100 mg of the powders or three pieces of the MMMs, were heated to 120 °C in an oven. In the final step, 50 mg of the powders or one piece of the MMMs was placed back in the crystallization dish with a screw lid glass filled containing concentrated hydrogen chloride to expose them to a hydrogen chloride atmosphere.

2.7 Characterization methods

NMR spectroscopy was conducted at room temperature at 400 MHz by using a Bruker BioSpin. The samples were dissolved in 0.6 mL 1 M $(NH_4)_2CO_3$ solution in D_2O under stirring overnight. The analysis of the spectra was realized by TopSpin 4.0.9 software.

Emission spectra of the samples were recorded using a Horiba Scientific FluoroMax-4 with Hellma Analytics High Precision Cells having a light path of 0.01 mm. The samples were excited at 296 nm and a 400 nm emission filter was used during the measurement.

Emission spectra were also detected with a portable fluorescence spectrometer called Indigo from GoyaLab. The samples were placed in a self-designed and 3D-printed measuring cell with two gas ports to enable a measurement under nitrogen flow. The samples were covered with a 3D-printed mask and the Indigo was placed on top of the mask. The excitation was performed with a wavelength of 300 nm.

IR spectra were measured using a Bruker Vertex 70v equipped with an ATR unit. The measurements were carried out under vacuum.

Powder X-ray diffraction (PXRD) was carried out by using a Stoe Stadi P transmission diffractometer operating with Ge (111)-monochromatized $CuK_{\alpha 1}$ radiation (λ = 1.54056 Å) and a position sensitive Mythen 1K Detector.

Argon physisorption isotherms were measured at 87 K using a Micromeritics 3Flex instrument. The powder samples were outgassed at 120 °C while the modified MMMs were outgassed at 60 °C in vacuum immediately prior the measurement. The determination of the BET surface area was realized by the 3Flex Version 5.02 software enabling the assessment of the relative pressure range for BET according to the Rouquerol plot. The pore width distribution was also investigated by NLDFT for cylindrical pore geometry.

Water physisorption isotherms were recorded at 298 K by a 3P instrument. The samples were outgassed at 120 °C (powders) or 60 °C (MMMs), respectively, in vacuum immediately prior to the measurement.

SEM measurements were performed on a Hitachi Regulus 8230 scanning electron microscope using secondary electrons at 2 kV. The used working distance was around 10 mm. Cross-sectional images were also taken at 2 kV and a working distance of 10 mm. EDX spectra were measured with the integrated EDX-detector Oxford UltiMAX 100 in mapping mode with a working distance of 10 mm and measurement time of 10 min. The data were quantitatively evaluated in the Aztec Version 6.0 software from Oxford Instruments.

The samples were fixed on a holder with carbon tape. For cross section images, the MMMs were fixed on silicon wafers with carbon tape and were placed into a cross section holder.

The samples were measured before and after the read-out sequence as powders or MMMs, respectively, *via* UV-vis spectroscopy in the range from 300 to 800 nm. The measurements were performed on a Cary4000 from Agilent Technologies by using a Praying Mantis Diffuse Reflection Accessory from Harrick.

The XPS measurements were performed using a Versaprobe III instrument from Physical Electronics equipped with an Al anode (1487.7 eV, 50 W, 15 kV) with an X-ray spot size of 200 μm in diameter and dual-beam charge neutralization during analysis. The acquired data was shifted using the C 1s signal of carbon, processed and evaluated using the MultiPak Software (ULVAC-PHI).

3. Results and discussion

3.1. Characterization of MOF-808 as starting material

Several batches of MOF-808 were synthesized at a gram scale according to the previous literature.[20] In this work, only acetic acid was used for the modulated synthesis of the framework. The resulting white powders show not only high crystallinity as determined by PXRD (see ESI Fig. S1), but also high porosity as confirmed by argon sorption measurements (see ESI Fig. S2†). The material exhibits a BET surface area of 1940 $m^2 g^{-1}$ and a pore width of 17 Å which corresponds to the isotherm displaying two steps. The second step is characteristic for the larger micropores of MOF-808. The accessibility of the pore system is crucial for the subsequent modification step.

Another important feature of MOF-808, relevant to its purpose of incorporating metal cations into the framework, is that only half of the coordination sites at the IBUs are occupied by linker molecules. This leaves the remaining sites available for coordination by modulators from the synthesis, water molecules, hydroxides, chlorides, or post-synthetic metal

cation insertion. To ensure comparable properties across different batches, we analyzed material compositions using ^{1}H-NMR spectroscopy (see ESI Fig. S3†). The analysis revealed that the number of acetates installed at the IBUs of MOF-808 ranges from 3.3 to 3.7 per Zr_6 cluster, indicating that all analyzed batches of MOF-808 have approximately two unsaturated sites that may be coordinated with metal cations without the need for prior modulator exchange.

3.2. Insertion of transition metals into MOF-808

In order to design a barcode material exhibiting visible color change and fluorescence switching by ligand exchange, the first step is to transform the white MOF-808 powder into a colored material. This was realized by post-synthetic modification (PSM) with transition metal cations by adding $CoCl_2{\cdot}6H_2O$ or $FeCl_2{\cdot}4H_2O$, to MOF-808 powder in *N*,*N*-dimethylformamide at 60 °C for 24 h. The modified MOF-808 materials are hereafter referred to as TM-MOF-808 (TM = transition metal). The color change of the starting material visibly indicates the successful insertion of transition metal cations at the IBUs of MOF-808. Cobalt cation insertion results in a blue powder product, while iron cation insertion forces the material to change color to orange-brown (see Fig. 1). Transition metal incorporation induced color changes can also be detected using UV-vis spectroscopy (see ESI Fig. S4†). No structural changes were observed after the PSM and the materials' crystallinity remains excellent (see Fig. 1).

The amount of introduced transition metal cations in relation to the Zr_6 clusters was determined using EDXS measurements. Fe-MOF-808 exhibits ≈1.6 iron cations per Zr_6 cluster. In contrast, only ≈0.7 cobalt cations per Zr_6 cluster could be introduced. As described by Castillo-Blas *et al.*,[15] the introduced iron cations are able to form Fe-oxo dimers bridging two adjacent Zr_6 clusters in MOF-808, which could provide an explanation for the higher possible loading with metal cations.

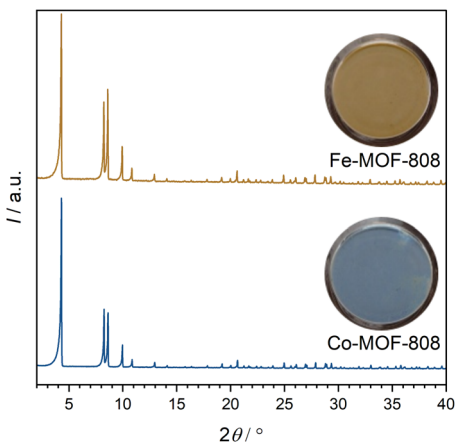

Fig. 1 PXRDs of Fe- (top) and Co-MOF-808 (bottom) with photographs of the powders in glass vials.

3.3. Insertion of lanthanide cations into MOF-808

Lanthanide cations were added to MOF-808 to design a material that exhibit switchable fluorescence behavior. This strategy takes advantage of the antenna effect of the linker molecule H_3btc which is known to enhance the fluorescence properties of lanthanide cations by efficient energy transfer. Therefore, the starting material was soaked for 24 h at room temperature in an acetone solution containing an amount of $Eu(NO_3)_3{\cdot}6H_2O$ that could potentially saturate all sites of the IBU that are not coordinated by linkers. The XRD analysis of the material (see ESI Fig. S5†) confirmed that this post-synthetic modification did not alter the structure of the starting material.

While previous studies have reported that MOF-808 containing europium[16] or terbium cations,[6] exhibits intense fluorescence under UV excitation due to the antenna effect of H_3btc on the lanthanide cations, our as-synthesized Eu-MOF-808 did not display such fluorescence that could be perceived by the naked eye (see Fig. 2a). Despite this, XPS (see ESI Fig. S6†) and EDXS analyses have confirmed the successful incorporation of europium into MOF-808. Interestingly, these measurements

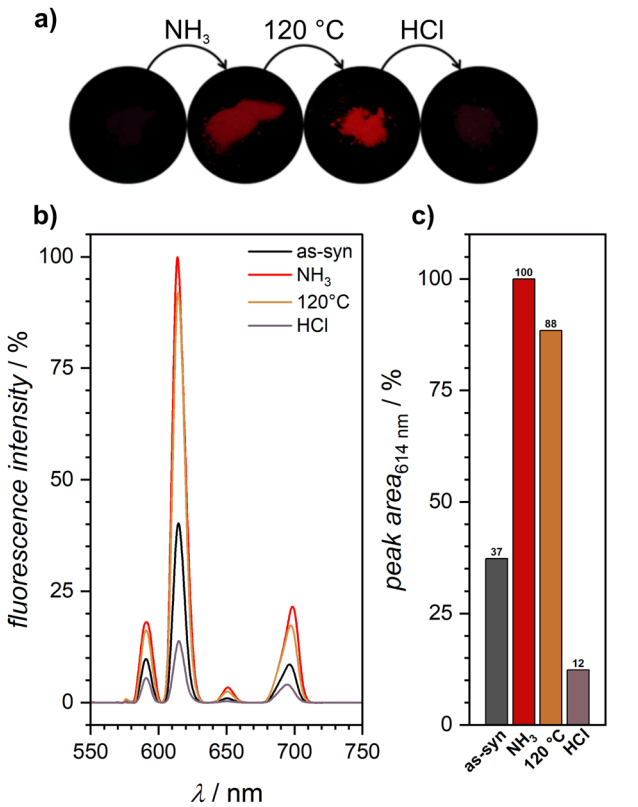

Fig. 2 (a) Fluorescence switching of as-synthesized Eu-MOF-808 caused by a sequence of chemical and thermal treatment. NH_3 exposure causes the *turn-on* of the fluorescence which remains also after activation at 120 °C. HCl exposure leads again to the total *turn-off* of the fluorescence, (b) emission spectra (λ_{ex} = 300 nm) of as-synthesized Eu-MOF-808 before and after all steps of the read-out sequence measured under ambient conditions, (c) comparison of the relative peak areas of the strongest peaks at 614 nm under the various treatments, normalized to the peak area of the ammonia exposed sample, which is set to 100%.

indicated a low incorporation rate, with only 0.2 europium cations per Zr_6 cluster being integrated. Nevertheless, we found a procedure to enable this minimal europium content to result in a material exhibiting pronounced fluorescence. These procedures are elaborated in the following section.

3.4. Targeted fluorescence switching of Eu-MOF-808 by chemical and thermal stimuli

Since the creation of a barcode capable not only of stationary information encoding but also of dynamic encoding is desirable, it is necessary to define a sequence based on chemical and thermal stimuli that enables the selective switching of fluorescence. This should be expressed in the targeted *turn-on* or *turn-off* of the fluorescence after the respective sequence step, so that the multi-step sequence has to be applied before the complete read-out of the barcode is possible.

3.4.1. Fluorescence *turn-on* by ammonia exposure. In the literature, there are several reports that europium complexes and europium-based MOFs undergo fluorescence quenching when the europium cations are coordinated by water molecules due to the unwanted energy transfer to their third vibrational overtones (3300–3500 cm^{-1}).[22] Given that MOF-808 possesses hygroscopic properties, and the introduction of europium maintains this characteristic, it is evident that europium interacts with water molecules in the as-synthesized samples. This is corroborated by the IR spectra, which clearly show the presence of water within the MOF after synthesis (see Fig. 3). We monitored the fluorescence intensity of our as-synthesized Eu-MOF-808 in dependence of relative humidity to investigate the extent to which water affects the fluorescence (see ESI Fig. S7†). Our observation revealed a drastically reduced fluorescence intensity with increasing relative humidity, with the fluorescence of the as-synthesized material almost halved at relative humidity above 50%.

It is noteworthy that ammonia has been reported as an efficient reagent to counteract the quenching effect caused by OH-vibrations by forming strong $NH_3{\cdot}H_2O$ bonds with water molecules that coordinate to the europium cations in the complexes. This effectively weakens the bond strength of the water molecule with europium, resulting in fluorescence *turn-on*.[23,24]

Motivated by this insight, we exposed the non-fluorescent, as-synthesized Eu-MOF-808 to gaseous ammonia. Despite the low amount of introduced europium cations, this treatment resulted in fluorescence *turn-on* of the material, enhancing the fluorescence intensity in comparison to the as-synthesized material (see Fig. 2). The resulting fluorescence spectrum (see Fig. 4) shows sharp emission peaks characteristic for europium cations. The spectrum shows five peaks at 578 nm, 591 nm, 614 nm, 650 nm, and 699 nm, with the peak at 614 nm being the most intense. The emission peaks result from the energy transfer from the triplet state of the btc^{3-} linker molecule to the excited state of europium, $^5D_0$, and the further transition to the ^7F_J (J = 0–4) states.[25]

To prove that the *turn-on* was caused by the coordination of ammonia molecules, FTIR spectra were recorded (see Fig. 3). After exposure to ammonia, two new peaks appear at ≈3200 cm^{-1} and ≈3000 cm^{-1}, which can be attributed to the

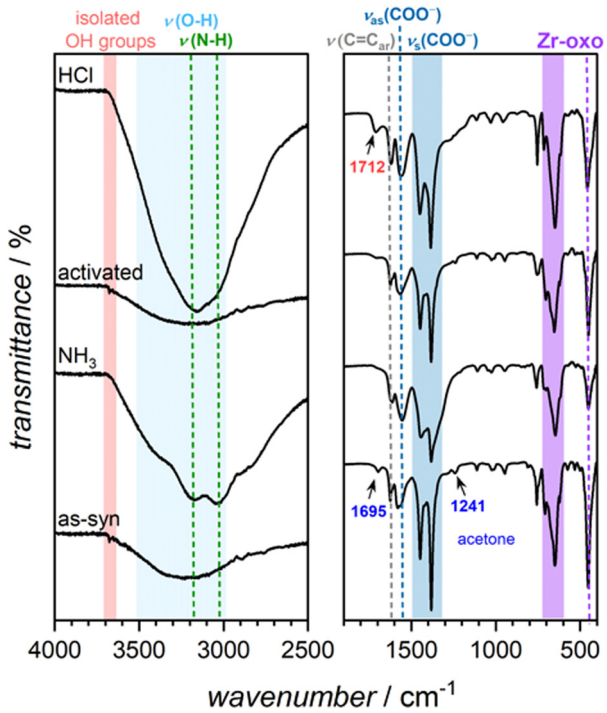

Fig. 3 IR spectra of Eu-MOF-808 from bottom to top before (as-syn) and after the sequence steps of ammonia exposure, activation at 120 °C and HCl treatment.

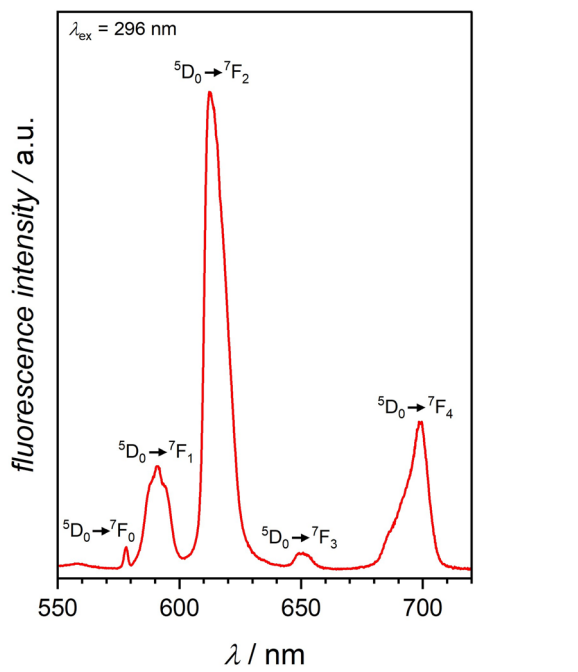

Fig. 4 Emission spectrum of Eu-MOF-808 after NH_3 exposure showing sharp peaks at 578 nm, 591 nm, 614 nm, 650 nm, and 699 nm. The excitation of the sample was performed at 296 nm.

valence vibrations associated with ammonia. Additionally, a broad peak ranging from 3600 cm^{-1} to 3000 cm^{-1} indicates the presence of water. The water peak was already present in the spectrum of the as-synthesized material, but intensified after exposure to ammonia, suggesting that ammonia treatment also introduced water molecules. Mirochnik *et al.*[23] reported that even substantial humidity has no effect on fluorescence enhancement when ammonia is present. Furthermore, the peak at 3677 cm^{-1} caused by isolated OH groups at the IBUs of the framework[26] disappeared after ammonia exposure, indicating that hydrogen bonds were formed. This is consistent with findings by Sergeev *et al.*,[24] who point out that the direct substitution of water molecules in the coordination sphere of europium is implausible.

3.4.2. Activation of the material. To develop a fluorescence switching sequence, we aimed to turn off the fluorescence of the material in a subsequent step. After exposing the material to ammonia, it was activated at 120 °C to remove the molecules responsible for the *turn-on*. The absence of the N–H valence vibrations and the reappearance of signals from isolated OH groups in the FTIR spectrum (see Fig. 3) confirmed the removal of ammonia molecules. However, visually, there was no discernible change in fluorescence (see Fig. 2a). This aligns with the emission spectra, indicating only a 10% decrease in fluorescence intensity. Nevertheless, without the ammonia exposure step, the sole activation of the as-synthesized material is insufficient to initiate fluorescence *turn-on* (see ESI Fig. S8†).

3.4.3. Fluorescence *turn-off* by treatment with hydrogen chloride. Fluorescence *turn-off* in europium-containing materials can be induced through acid treatment with gaseous hydrogen chloride, as reported in the literature.[27] According to Gao *et al.*,[11] the protonation of water molecules and hydroxides coordinated to the europium sites could affect the surrounding electrons and could result in a reduction of fluorescence intensity. By treating Eu-MOF-808 with gaseous hydrogen chloride after the activation procedure, there was a visible decrease in fluorescence (see Fig. 2), which was confirmed by a reduction in fluorescence intensity to 12% in the emission spectrum. The treatment led to an increase of the water signal in the FTIR spectrum and a decrease of the signal caused by isolated OH groups (see Fig. 3). A distinct peak at ≈1712 cm^{-1} suggests protonation of modulators or water molecules. In contrast, the FTIR spectrum of unmodified MOF-808 (see ESI Fig. S9†) lacks these features after the similar treatment, indicating that the molecules coordinated to europium must be involved in the protonation process. This protonation may facilitate the introduction of water molecules that lead to the quenching of fluorescence.

The three mentioned steps (exposure to ammonia, activation at 120 °C, HCl treatment) were defined as a multi-step read-out sequence that allows the precise on and off switching of the fluorescence of the as-synthesized Eu-MOF-808. The activation step was included to prevent ammonium chloride formation, which could occur if the hydrogen chloride treatment was performed immediately after the ammonia exposure. As evident from the PXRDs (see ESI Fig. S5†), Eu-MOF-808 maintains its crystallinity throughout all the steps of the sequence.

3.5. Combined incorporation of transition metal and lanthanide cations into the same framework

Both optical properties, fluorescence and color, of Eu- and TM-MOF-808 have been combined in a single material: initially, MOF-808 was functionalized with transition metals to achieve a colored material using previously described methods. Afterwards, europium cations were incorporated to obtain Eu,TM-MOF-808. The introduction of europium cations did not alter the crystallinity and structure (see ESI Fig. S10†).

Compared to MOFs that contain solely transition metal cations, the materials exhibited a less intense color. This decrease in intensity can be attributed to the competition between the later-added europium cations and the transition metal cations for coordination sites at the IBUs. The observed reduction in the concentration of transition metal cations within the framework suggests that they are displaced by the europium cations. This conclusion is supported by EDXS measurements, which confirmed a decrease in the content of transition metal cations. Specifically, the quantities of cobalt and iron cations decreased to 0.2 and 0.4 per Zr_6 cluster, respectively. Conversely, in comparison to pure Eu-MOF-808, a larger amount of europium cations was observed (≈0.6 Eu:Zr_6).

Argon sorption measurements of Eu,TM-MOF-808 samples showed that the BET surface areas were reduced compared to MOF-808 (see ESI Fig. S2 and S11†). However, despite this reduction, the materials maintained high porosities, allowing guest molecules to enter the pore system. This suggests that our defined sequence is still suitable for these materials. Each step in our sequence was applied for one hour to ensure complete exposure of the entire powder sample in that step.

3.5.1. Read-out sequence of Eu,Co-MOF-808. Upon exposure to ammonia, Eu,Co-MOF-808 undergoes a color change from blue to pink (see Fig. 5, top left). This is further confirmed by the UV-vis spectroscopy findings (see ESI Fig. S12†). In addition, the sample shows a fluorescence *turn-on* (see Fig. 5, bottom left) as expected. FTIR spectra for both as-synthesized and ammonia-exposed samples are remarkably like those of Eu-MOF-808, with no distinguishable differences in vibration peaks (see ESI Fig. S13†).

After activation of the sample at 120 °C, Eu,Co-MOF-808 turns blue, indicating NH_3 ligand removal from the transition metal centers. However, the FTIR spectrum shows incomplete removal of ammonia molecules upon heating. Interestingly, fluorescence of the MOF is initially suppressed after activation (see Fig. 5), which is different from the fluorescence response of Eu-MOF-808 after this step. This suggests that the incorporated cobalt cations significantly influence the fluorescence of europium, which can be explained by Förster Resonance Energy Transfer (FRET) between europium and cobalt, which leads to luminescence quenching. Thus, the quenching of the fluorescence by excitation of the d–d transitions of cobalt can be observed because the wavelength range of europium emis-

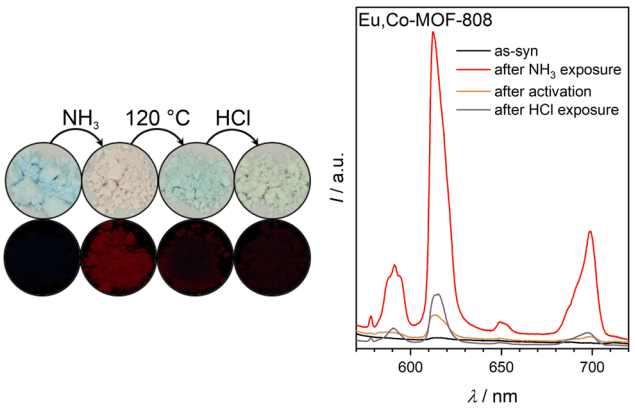

Fig. 5 Color changes based on ligand exchange and fluorescence switching recorded under UV light (254 nm, left) and fluorescence spectra of as-synthesized Eu,Co-MOF-808 (λ_{ex} = 296 nm, right) before and after all steps of the read-out sequence measured under ambient conditions.

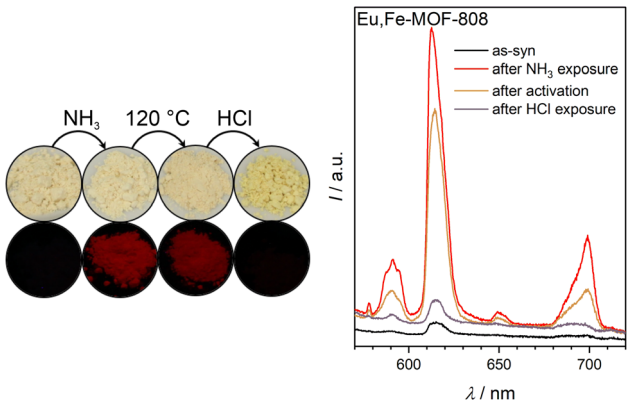

Fig. 6 Color changes based on ligand exchange and fluorescence switching recorded under UV light (254 nm, left) and fluorescence spectra of as-synthesized Eu,Fe-MOF-808 (λ_{ex} = 296 nm, right) before and after all steps of the read-out sequence measured under ambient conditions.

sion (see Fig. 5) perfectly aligns with the absorption spectrum of the cobalt containing material (see ESI Fig. S12†).

Interesting to note, the fluorescence of the material gradually returns (see ESI Fig. S14†), with a color change to light-pink under ambient conditions. This indicates that environmental humidity has a profound influence on the fluorescence behavior which will be further discussed later.

The third step of the read-out sequence, the treatment with gaseous HCl, results in Eu,Co-MOF-808 changing its color to blue-green. After this treatment, the fluorescence of the sample is turned off (see Fig. 5). The FTIR spectrum (see ESI Fig. S13†) suggests protonation of modulators or water molecules, which has been previously observed for Eu-MOF-808 (compare 3). It is possible that the inhibition of the host–guest hydrogen bonding interactions[28] due to protonation is responsible for the fluorescence quenching in Eu,Co-MOF-808.

3.5.2. Read-out sequence of Eu,Fe-MOF-808. Contrary to Eu,Co-MOF-808, Eu,Fe-MOF-808 does not show any visible color change upon exposure to ammonia and remains light orange while the fluorescence is still turned on in this step (see Fig. 6, top). Even after the activation process at 120 °C, the color of the MOF remains unchanged. The fluorescence is slightly reduced by this procedure (see Fig. 6, bottom), mirroring the pattern observed in Eu-MOF-808.

Notably, again the activation does not fully expel the ammonia molecules, as can also be seen in the FTIR spectrum (see ESI Fig. S13†). The FTIR spectra of this MOF lack the peak associated with the vibration of isolated OH groups. This suggests potentially higher water loading in Eu,Fe-MOF-808.

During the third step of the read-out sequence, the treatment with gaseous HCl makes Eu,Fe-MOF-808 displaying a yellow-colored powder. After this procedure, the fluorescence of the sample is turned off (see Fig. 6). The FTIR spectrum of the material (see ESI Fig. S13†) further underscore protonation, as already described for Eu-MOF-808 (compare 3).

3.5.3. Influence of humidity on europium fluorescence depending on the present transition metals. To further investigate the effect of the humidity on the fluorescence performance of the materials, taking into account the incorporated transition metal cation, we performed fluorescence measurements at different relative humidities of as-synthesized Eu,TM-MOF-808. Compared to the as-synthesized Eu-MOF-808 (see ESI Fig. S7†), the MOF containing cobalt displays substantial fluorescence *turn-on* at higher relative humidities (see Fig. 7), with the highest increase between 20% and 30% RH. This fluorescence increase profile correlates perfectly with the water uptake of the MOF as determined by water sorption (see Fig. 8, left). This confirms that the rise in fluorescence is linked to adsorbed water content. In contrast, the water sorption isotherm of the iron containing MOF does not correlate with the fluorescence measurements (see Fig. 8, right). Nevertheless, the diminished fluorescence can be

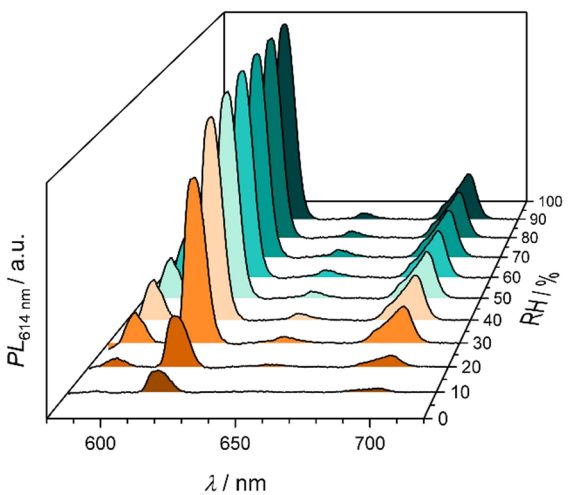

Fig. 7 Emission spectra of Eu,Co-MOF-808 at different relative humidities showing an increasing fluorescence intensity with higher relative humidities.

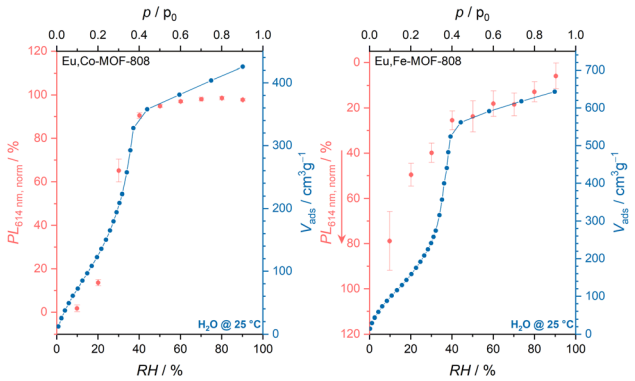

Fig. 8 Comparison of fluorescence intensities of Eu,Co- (left) and Eu,Fe-MOF-808 (right) at different relative humidities with the water uptake monitored by water sorption measurements.

associated with a higher amount of adsorbed water molecules in line with the behavior of Eu-MOF-808. Thus, the incorporation of cobalt cations has a significant stronger influence on the fluorescence of the material than iron cations.

Many humidity sensors based on europium compounds have been observed to exhibit varying responses to humidity: while a decrease in fluorescence with increasing humidity is common,[29–33] there are also reports of materials showing the opposite tendency.[28,34] The persistence of fluorescence in the presence of increasing amounts of water molecules could be justified by an efficient reduction of the strong coupling of O–H vibrations on the water molecules coordinating to europium within the framework by host–guest O–H···O hydrogen bonding interactions.[28]

Further research is needed to clarify these observations, specifically regarding the positions of transition metal and europium cations in the framework and to understand the underlying reasons for such metal-specific influences. However, this would require, for example, XAFS measurements at the synchrotron, which could not be realized within the scope of this work.

3.6. Preparation of mixed-matrix membranes

To improve the handling of the powder samples for their application as barcode materials, we prepared mixed-matrix membranes (MMMs). Therefore, the synthesized TM-MOF-808 powders were incorporated into a polyvinylidene fluoride (PVDF) matrix. The powders were first dispersed in acetone, undergoing ultra-sonification for 30 min. Subsequently, a solution of PVDF in DMF was added to the dispersion. The mixture was ultrasonicated for another 30 min. After removing the solvent under reduced pressure, the viscous mixture was spread on a glass slide using a doctor blade technique. The applied material was then dried at 70 °C for 1 h, resulting in the formation of the mixed-matrix membrane.

The mixed-matrix membranes retained the high crystallinity of the powder samples, as confirmed by PXRD measurements (see ESI Fig. S15†). SEM images demonstrate the homogeneous integration of octahedral MOF particles into the polymer matrix (see Fig. 9). The thicknesses of different batches of mixed-matrix membranes were determined by cross section images and varied from approx. 30 nm to 70 nm (see ESI Fig. S16†), primarily due to the manual application using the doctor blade.

Regarding the composition of the MMMs, we determined MOF loading by immersing a defined amount of MMM in DMSO, followed by the addition of hydrogen fluoride for 24 h to dissolve the MOF particles. Pure PVDF was left after this process, and the resulting mass difference allowed us to calculate the MOF content, which ranged from 50 to 70 wt% (see ESI Fig. S16†).

For the introduction of lanthanide cations, uniformly sized pieces of the MMM were immersed in an europium(III) nitrate hexahydrate solution in acetone. After only 10 min, we obtained the modified MMM, which we now refer to as Eu,TM-MOF-808@PVDF. Notably, the porosities of these materials decreased compared to the powder samples as a consequence of their incorporation into the PVDF matrix (see ESI Fig. S17†).

The MMMs underwent the same read-out sequence with an exposure time of 10 min per step. The color changes and fluorescence switching caused by the read-out sequence (see Fig. 10) were comparable to those observed for the powder samples. PVDF, the polymer used, showed no fluorescence after being soaked in the mentioned europium-containing solution and exposure to ammonia (see ESI Fig. S18†). Additionally, the MMM samples also remain structural intact after each read-out step (see ESI Fig. S19†).

The fluorescence read-out of the MMMs was performed with a portable fluorescence spectrometer. The measurement setup is described in more detail in the ESI.† To ensure a consistent basis for comparison, the absolute fluorescence intensities of the materials were normalized. For this purpose, the areas of the peaks at 614 nm of the samples were determined

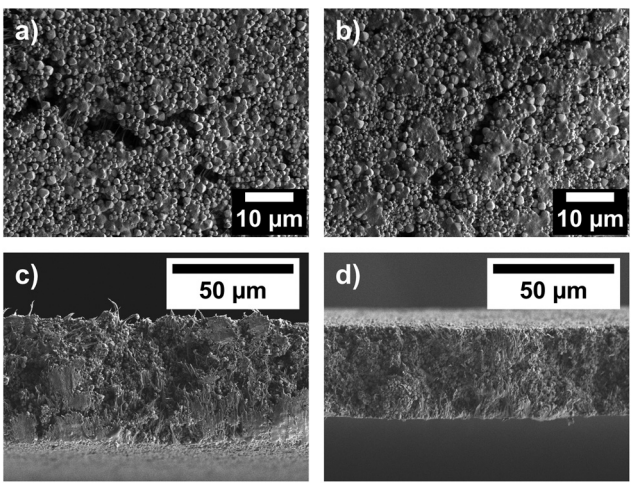

Fig. 9 Top view SEM images of (a) Co- and (b) Fe-MOF-808@PVDF, as well as cross-section SEM images of (c) Co- and (d) Fe-MOF-808@PVDF.

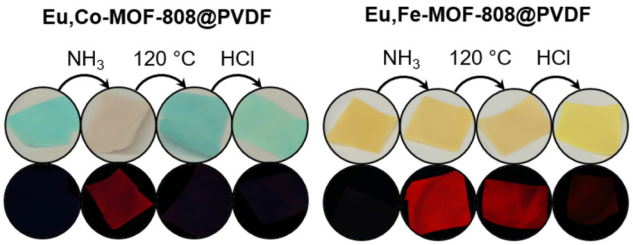

Fig. 10 Illustration of the visible color changes (top) and the fluorescence switching (bottom, λ_{ex} = 254 nm) of the Eu,TM-MOF-808@PVDF.

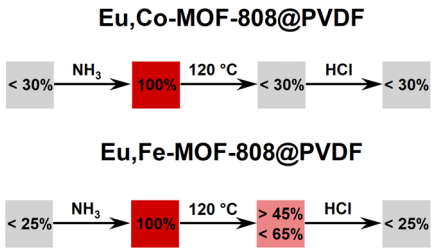

Fig. 11 Defined read-out sequence and the expected responses of the respective materials.

after every read-out step and referenced to the peak area of the sample exposed to ammonia, so that this sample always corresponds to 100% and serves as a standard. In addition to this, the fluorescence spectra underwent background correction to improve accuracy. This method ensures comparable fluorescence values regardless of the MMM batch used.

The fluorescence results show high consistency, across different batches of MMM (MMM 1–4) used for the modification and different modification batches of the same MMM (see ESI Fig. S21†). Based on the obtained measurement results for every read-out step, reproducible response ranges of the respective materials could be defined as shown in Fig. 11.

It must be emphasized here that the read-out response defined for the activation step in the case of Eu,Fe-MOF-808 refers to the intensity, which stabilizes at a minimum value. This equilibrium intensity level will not decrease further, regardless of the read-out time after the sequence application. The immediate read-out after activation leads to higher intensity values (see ESI Fig. S22†) yet the sample is still in the switched-on state. However, this equilibrium read-out value can also be achieved by treating the sample with a moistened gas stream, which reduces the fluorescence intensity to this stable minimum, as demonstrated in Fig. S22 in the ESI.†

Because of the successful control of the visible color change and the fluorescence switching through the mentioned read-out sequence, Eu,TM-MOF-808@PVDF presents a promising option for barcode material. In order to design barcodes, different modified MMM pieces can be arranged into specific patterns. An exemplary pattern and its read-out process are shown in Fig. S23 in the ESI.† Moreover, our approach allows the creation of more complex patterns as demonstrated in Fig. 12. This increased complexity is attained using both europium modified and unmodified TM-MOF-808@PVDF pieces (see ESI Fig. S24†).

These pieces show the same color changes, but only the europium modified ones exhibit fluorescence switching. For instance, we assembled the number “80” using both types of pieces. The number remains visible throughout the entire read-out process, while only the colors of the pieces change.

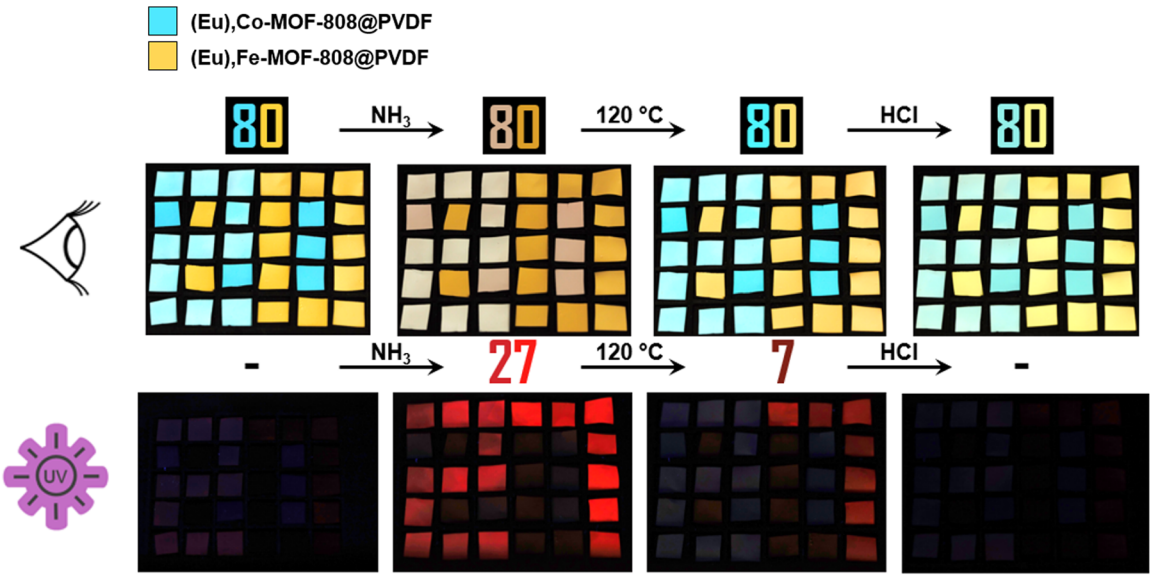

Fig. 12 Barcode pattern design. With naked eye, only the color change of “80” can be observed after every sequence step. Under UV light, the number “27” appears after ammonia exposure while only “7” remains after the heating step. In addition to the visible “80”, the code also includes “27” and “7”. Thus, the complete coded number is “80277”.

Interestingly, under UV light, different numbers become visible at different stages due to selective fluorescence switching in the modified pieces. No number is visible initially, but after ammonia exposure, the number "27" appears under UV-light. The fluorescence after the activation step depends on the transition metal incorporated, resulting in only the number "7" remaining. Finally, the last step causes the numbers to disappear revealing that the apparent code is "80" while the hidden code is "80277".

4. Conclusions

In conclusion, we were able to construct a barcode prototype capable of defined and reproducible visible color changes and fluorescence switching triggered by a multi-step read-out sequence. The barcode material is based on MOF-808 powder modified with cobalt or iron cations, respectively, which is embedded into polyvinylidene fluoride to form mixed-matrix membranes. The mixed-matrix membranes afterwards were modified with europium cations responsible for the sharp emission spectra of the materials. The read-out sequence is defined into three steps: exposure to ammonia, activation at 120 °C and treatment with hydrogen chloride. Each step plays a crucial role in initiating the essential optical und fluorescence features of the barcode.

Looking beyond the technical aspects of this study, the potential implications are significant. The sensitivity of the barcode to various environmental stimuli, combined with its unique visual and fluorescent reactions, creates opportunities for its use in fields such as secure data encryption, anti-counterfeiting measures and advanced sensing technologies. The versatility of the MOF-based system and tunable read-out sequence offer a customizable platform that can be adapted to various needs. This study demonstrates a substantial advancement in optical encoding and smart material applications.

Conflicts of interest

There are no conflicts to declare.

Acknowledgements

General support and fruitful discussions with Prof. Dr Peter Behrens are gratefully acknowledged. The authors would like to thank the Hannover School for Nanotechnology (hsn) which is based in the Laboratory for Nano and Quantum Engineering (LNQE) for financial funding.

References

1 K. Jiang, Y. Wang, C. Lin and H. Lin, *Adv. Mater.*, 2018, **30**, 1800783.
2 J. Y. R. Silva, L. L. Da Luz, F. G. M. Mauricio, I. B. Vasconcelos Alves, J. N. d. S. Ferro, E. Barreto, I. T. Weber, W. M. de Azevedo and S. A. Júnior, *ACS Appl. Mater. Interfaces*, 2017, **9**, 16458–16465.
3 P. Kumar, S. Singh and B. K. Gupta, *Nanoscale*, 2016, **8**, 14297–14340.
4 H. Wang, D. Zhao, Y. Cui, Y. Yang and G. Qian, *J. Solid State Chem.*, 2017, **246**, 341–345.
5 Y. Lu and B. Yan, *J. Mater. Chem. C*, 2014, **2**, 7411–7416.
6 J. Zhang, S. B. Peh, J. Wang, Y. Du, S. Xi, J. Dong, A. Karmakar, Y. Ying, Y. Wang and D. Zhao, *Chem. Commun.*, 2019, **55**, 4727–4730.
7 Y. Cui, B. Chen and G. Qian, *Coord. Chem. Rev.*, 2014, **273–274**, 76–86.
8 K. A. White, D. A. Chengelis, K. A. Gogick, J. Stehman, N. L. Rosi and S. Petoud, *J. Am. Chem. Soc.*, 2009, **131**, 18069–18071.
9 J. I. Deneff, K. S. Butler, L. E. S. Rohwer, C. J. Pearce, N. R. Valdez, M. A. Rodriguez, T. S. Luk and D. F. Sava Gallis, *Angew. Chem., Int. Ed.*, 2021, **60**, 1203–1211.
10 Z. Gao, B. Xu, T. Zhang, Z. Liu, W. Zhang, X. Sun, Y. Liu, X. Wang, Z. Wang, Y. Yan, F. Hu, X. Meng and Y. S. Zhao, *Angew. Chem., Int. Ed.*, 2020, **59**, 19060–19064.
11 J.-P. Gao, R.-X. Yao, X.-H. Chen, H.-H. Li, C. Zhang, F.-Q. Zhang and X.-M. Zhang, *Dalton Trans.*, 2021, **50**, 1690–1696.
12 Y. Zhang, X. Xu and B. Yan, *J. Mater. Chem. C*, 2022, **10**, 3576–3584.
13 H. Furukawa, F. Gándara, Y.-B. Zhang, J. Jiang, W. L. Queen, M. R. Hudson and O. M. Yaghi, *J. Am. Chem. Soc.*, 2014, **136**, 4369–4381.
14 E. Aunan, C. W. Affolter, U. Olsbye and K. P. Lillerud, *Chem. Mater.*, 2021, **33**, 1471–1476.
15 C. Castillo-Blas, I. Romero-Muñiz, A. Mavrandonakis, L. Simonelli and A. E. Platero-Prats, *Chem. Commun.*, 2020, **56**, 15615–15618.
16 X. Zhang, Y. Li and L. Zhang, *Spectrochim. Acta, Part A*, 2021, **251**, 119464.
17 W. Jumpathong, T. Pila, Y. Lekjing, P. Chirawatkul, B. Boekfa, S. Horike and K. Kongpatpanich, *APL Mater.*, 2019, **7**, 111109.
18 S. Schmitz, N. V. Izarova, J. van Leusen, K. Kleemann, K. Y. Monakhov and P. Kögerler, *Inorg. Chem.*, 2021, **60**, 11599–11608.
19 X. Liu, K. O. Kirlikovali, Z. Chen, K. Ma, K. B. Idrees, R. Cao, X. Zhang, T. Islamoglu, Y. Liu and O. K. Farha, *Chem. Mater.*, 2021, **33**, 1444–1454.
20 N. Marquardt, M. Dahlke and A. Schaate, *ChemPlusChem*, 2023, **88**, e202300109.
21 M. S. Denny, M. Kalaj, K. C. Bentz and S. M. Cohen, *Chem. Sci.*, 2018, **9**, 8842–8849.
22 A. Beeby, I. M. Clarkson, R. S. Dickins, S. Faulkner, D. Parker, L. Royle, A. S. de Sousa, J. A. G. Williams and M. Woods, *J. Chem. Soc., Perkin Trans. 2*, 1999, 493–504.
23 A. G. Mirochnik, N. V. Petrochenkova, A. S. Shishov, B. V. Bukvetskii, T. B. Emelina, A. A. Sergeev and

S. S. Voznesenskii, *Spectrochim. Acta, Part A*, 2016, **155**, 111–115.
24 A. A. Sergeev, S. S. Voznesenskiy, N. V. Petrochenkova, A. S. Shishov, A. A. Leonov, T. B. Emelina, A. G. Mirochnik and Y. N. Kulchin, *Proc. SPIE - Int. Soc. Opt. Eng.*, 2016, **10176**, 1017610.
25 K. Müller-Buschbaum, F. Beuerle and C. Feldmann, *Microporous Mesoporous Mater.*, 2015, **216**, 171–199.
26 J. H. Cavka, S. Jakobsen, U. Olsbye, N. Guillou, C. Lamberti, S. Bordiga and K. P. Lillerud, *J. Am. Chem. Soc.*, 2008, **130**, 13850–13851.
27 X. Li, Y. Xie, B. Song, H.-L. Zhang, H. Chen, H. Cai, W. Liu and Y. Tang, *Angew. Chem., Int. Ed.*, 2017, **56**, 2689–2693.
28 Y. Yu, J.-P. Ma and Y.-B. Dong, *CrystEngComm*, 2012, **14**, 7157–7160.
29 Z. Wang, G. Sun, J. Chen, Y. Xie, H. Jiang and L. Sun, *Chemosensors*, 2022, **10**, 66.
30 Y. Gao, P. Jing, N. Yan, M. Hilbers, H. Zhang, G. Rothenberg and S. Tanase, *Chem. Commun.*, 2017, **53**, 4465–4468.
31 M. Li, Q. Lyu, L. Sun, B. Peng, L. Zhang and J. Zhu, *ACS Appl. Mater. Interfaces*, 2020, **12**, 39665–39673.
32 W. Zhang, J. Xie, Z. Sui, Z. Xu, X. Wang, M. Lei, H. Zhang, Z. Li, Y. Wang, W. Liu, W. Du and S. Wang, *Sci. China: Chem.*, 2021, **64**, 1723–1729.
33 D. Xia, J. Li, W. Li, L. Jiang and G. Li, *J. Lumin.*, 2021, **231**, 117784.
34 D. Wang, Q. Tan, J. Liu and Z. Liu, *Dalton Trans.*, 2016, **45**, 18450–18454.